Research Article | Vol. 29, No. 3 / 1 February 2021 / Optics Express 3764
Optics EXPRESS

Spectral shaping of ring resonator transmission response

MUKESH YADAV,* JONG WOOK NOH, DAG ROAR HJELME, AND ASTRID AKSNES

Department of Electronic Systems, Norwegian University of Science and Technology (NTNU), Trondheim NO- 7491, Norway
mukesh.yadav@ntnu.no

Abstract: We present a Mach-Zehnder interferometer assisted ring resonator configuration (MARC) to realize resonator transmission spectra with unique spectral signatures and significantly large effective free spectral ranges. Transmission spectra with unique spectral signatures are generated by changing the angular separation between the through port and the drop port waveguides of the ring resonator (RR). These spectral signatures are comprised of several distinct resonance lineshapes including Lorentzian, inverse Lorentzian and asymmetric Fano-like shapes. One of the spectral signatures generated from the MARC device is utilized for the temperature sensing measurement to demonstrate a MARC-based sensor with high Q-factor and wide measurement range.

1. Introduction

Silicon ring resonator based optical devices are widely utilized for various applications such as optical filters [1,2], modulators [3], and sensors [4–8]. This can be mainly attributed to the combination of high index contrast platform and the availability of complementary metal–oxide–semiconductor (CMOS) fabrication technology [9]. A conventional RR consists of a closed loop waveguide and a bus waveguide. The bus waveguide evanescently couples light into the closed loop waveguide. When the optical path length of the closed loop waveguide is equal to an integer multiple of the source wavelength, light inside the loop interferes constructively and results in resonance. Ring resonators support multiple resonances. The separation between adjacent resonances is defined as the free spectral range and depends on the optical path length of the closed loop. A resonance lineshape of optical resonators is generally symmetric Lorentzian, and its linewidth determines the performances of RR-based filters and sensors.

In recent years, extensive research has been specifically devoted to the modification of the RR resonance lineshape [10–13]. By modification of the resonance lineshape, sharp, and asymmetric Fano lineshapes and square, triangular, sinusoidal shapes are realized. The sharpness and the asymmetry of the Fano lineshape define the sensitivity of the device and enable photonic sensors with high sensitivity and switches with low switching energy [14–16]. Tunability of the asymmetry in Fano resonance lineshapes enables the realization of reconfigurable optical filters [17]. Square, sinusoidal, and triangular shapes are relevant for optical filtering applications [11,18].

The above-mentioned resonance lineshapes are commonly realized by ring-coupled Mach-Zehnder interferometer (MZI) devices, and they can be divided into two categories. One configuration, all-pass ring resonator inserted into one arm of the MZI, is utilized to convert the phase response at the through port output into the intensity response. This resultant response is comprised of Fano resonances spaced by the RR free spectral range [10,17,19,20]. The Fano resonance lineshape can be tuned into different asymmetrical ones by using an active or passive component on one of the arms in the configuration. The other configuration, add-drop ring resonator inserted into one arm of the MZI, is designated to translate the phase response at

#415683 https://doi.org/10.1364/OE.415683
Journal © 2021 Received 23 Nov 2020; revised 17 Jan 2021; accepted 18 Jan 2021; published 22 Jan 2021

Optics EXPRESS

the drop-port output into the intensity response [11,18]. In addition to the ring-enhanced MZI configurations, a double injection configuration has been explored to realize intensity responses with sinusoidal, triangular and square shapes [12].

Throughout this paper, we shall use the terms 'lineshape'and 'transmission spectrum'for the shape of an individual resonance and the intensity response over a wavelength range including several resonances, respectively.

In this paper, we present a Mach-Zehnder interferometer assisted ring resonator configuration (MARC) to tailor the RR drop port phase response and the resulting transmission spectrum. The phase response at the drop port is altered by carefully designing a RR geometry, specifically the angular separation constituted by two bus waveguides in the immediate vicinity of the ring. By incorporating a particular angular separation in the MARC device, it produces transmission spectra with unique spectral signatures and significantly large effective free spectral ranges. These unique spectral signatures are comprised of several distinct lineshapes including Lorentzian, inverse Lorentzian and asymmetric Fano-like shapes. Furthermore, these unique spectral signatures in the transmission spectrum remain unchanged even when the spectrum is shifted. (Note: Tuning and control of individual resonance lineshapes are out of the scope of this paper.) The combination of this characteristic and the large effective free spectral range is experimentally verified and utilized for a temperature sensing experiment to demonstrate a MARC sensor with high Q-factor of 60,000 and 2-fold enhanced measurement range compared with the conventional RR.

2. Theoretical analysis of the MARC

A MARC device is comprised of a balanced MZI and an add-drop ring resonator as shown in Fig. 1. The aim of this study is to investigate the effect of an arbitrary angular separation, θ, between the through and the drop port waveguides on the MARC intensity response. To analyze the MARC intensity response, we first consider a RR with an arbitrary angular separation and investigate the effect of the angular separation on the drop port phase response. The drop port amplitude transmission response, t, of a RR with an arbitrary angular separation as shown in Fig. 2(a) is given as [21]:

$$t = -\frac{\sqrt{1-\gamma_1^2}\sqrt{1-\gamma_2^2}a_{\mathrm{d}}\exp[i(\psi\frac{\theta}{2\pi})]}{1-\gamma_1\gamma_2 a\exp[i(\psi)]}, \tag{1}$$

where $\psi = \frac{\omega}{c}n(2\pi r)$ is the round-trip phase shift, n is the effective refractive index, r is the ring radius, a is the single-pass amplitude transmission factor, $\gamma_1(\gamma_2)$ is the self-coupling coefficient of the coupler and a_d is the fraction of the round-trip amplitude transmission factor between the input and output coupler.

The phase of the transmitted light at the RR drop port, ϕ, is given as [21,22]:

$$\phi = \arctan\frac{Im[t]}{Re[t]} = \pi + \psi\frac{\theta}{2\pi} + \arctan\frac{\gamma_1\gamma_2\sin(\psi)}{1-\gamma_1\gamma_2 a\cos(\psi)}. \tag{2}$$

To simplify the numerical analysis in the following, all the ring resonators are assumed to be identical (r=30 μm), lossless (a=1) and critically coupled (γ_1=γ_2).

In the MARC, the balanced MZI is used to convert the phase change introduced by resonances at the drop port into a transmission intensity. The intensity transmission response, T_{out}, obtained from the MARC can be expressed as [11,13]:

$$T_{\mathrm{out}} = \frac{1}{4}[1+|t|^2+2|t|\cos\phi]. \tag{3}$$

Figure 2(b) presents the phase response at the drop port with different angular separations. The ring resonator with the angular separation of 180° is a conventional add-drop resonator

Optics EXPRESS

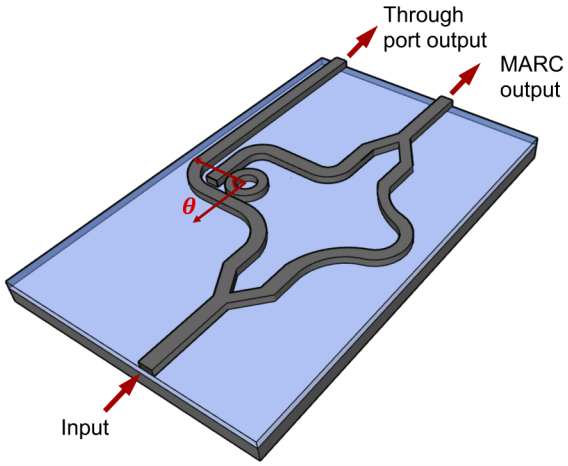

Fig. 1. Schematic of a MARC device with an angular separation of θ between the through port and the drop port waveguides.

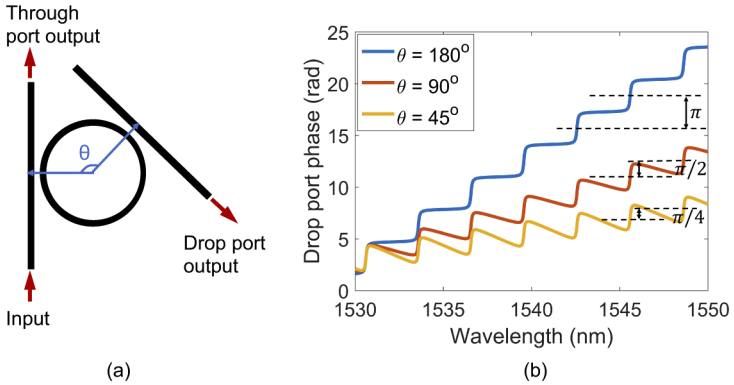

Fig. 2. (a) Schematic of a ring resonator with an angular separation of θ between the through port and the drop port waveguides, and (b) Drop port phase response for different angular separations.

configuration, and its phase increases monotonically as a function of wavelength, leading to π radians phase accumulation between resonances. For 90° angular separation, the accumulated phase difference between resonances is reduced to $\pi/2$ radians. The accumulated phase difference is further reduced to $\pi/4$ radians by setting the angular separation to 45°. The phase response at the drop port is a function of angular separation and wavelength, and thus it can be controlled by choosing a specific angular separation.

Figure 3 shows six transmission spectra of the MARC with angular separations of 180°, 135°, 90°, 60°, 45°, and 30°. The transmission spectrum for $\theta = 180°$ (Fig. 3(a)) is comprised of two distinct resonance lineshapes, separated by a free spectral range of 3 *nm*. These lineshapes exhibit Lorentzian and inverse Lorentzian resonance lineshapes corresponding to the interference maxima and minima. Figure 3(c) shows the transmission spectrum for $\theta = 90°$ with three distinct resonance lineshapes. These resonance lineshapes display Lorentzian, inverse Lorentzian and Fano-like shapes. The Fano-like lineshape is located in the middle of the Lorentzian and the inverse Lorentzian lineshapes, induced by the interference when the total phase accumulation is $\pi/2 + n\pi$. Furthermore, seven distinct resonance lineshapes are found in the transmission

Optics EXPRESS

spectrum of $\theta = 30°$ as depicted in Fig. 3(f), and five of them show asymmetric Fano-like shapes. Based on these transmission calculations, it is concluded that there is an inverse relationship between the angular separation and the number of distinct resonance lineshapes in a transmission spectrum. Consequently, a specific angular separation can be designated for a transmission spectrum in combination with multiple distinctive resonance lineshapes. Moreover, that makes it possible to have a unique spectral signature within a relatively narrow band.

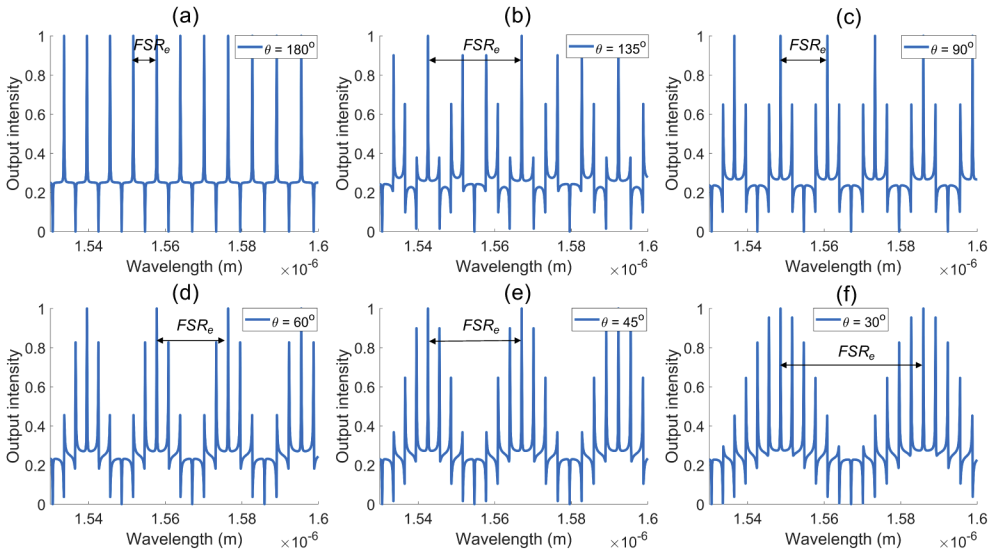

Fig. 3. Transmission spectra of MARC devices with angular separations of (a) 180°, (b) 135°, (c) 90°, (d) 60°, (e) 45°, and (f) 30°.

When the accumulated phase reaches an integer multiple of 2π, the resonance lineshape repeats itself. This results in a transmission spectrum with a certain period, defined as the effective free spectral range (FSR_e). The FSR_e is related to the free spectral range (FSR) of the given ring resonator. The FSR is defined as the separation between two consecutive resonances, and given by $\frac{\lambda^2}{n_g 2\pi r}$, where n_g is the group index, λ is the vacuum wavelength and r is the ring radius. For a given angular separation ($\theta = \frac{2\pi}{L}$), the FSR_e of a transmission spectrum can be expressed as,

$$FSR_e = N \cdot FSR, \tag{4}$$

where N satisfies the condition $\theta = 2\pi\frac{M}{N}$, that results in $L = \frac{N}{M}$, where N and M are integers. The parameter L can be divided into two cases. In one case, L is a rational number given as an irreducible fraction $L = \frac{p}{q}$, and its solutions are $N = p$ and $M = q$. In the other case, L is a positive integer, and its solutions N=L and M=1.

The effective free spectral range (FSR_e) for a given angular separation is governed by the positive integer N. The value of N is inversely proportional to the angular separation, which leads to an increase in the FSR_e. As shown in Fig. 3(f), the FSR_e is calculated to be 36 nm, and this is 12 times larger than the normal FSR of 3 nm. Figures 3(b) and (e) show that both spectra of 45° and 135° have the same FSR_e of 24 nm, but these spectra are highly distinctive. This phenomenon can be explained by the accumulated phase shift between the resonances. For the 135° case, the resonances occur with the phase shift of $\frac{3}{8}\pi$ radians, which is three times larger than that of the 45° case, and correspondingly this difference differentiates one transmission spectrum from another. However, both cases require the same number of phase-shift steps to attain the total phase accumulation of an integer multiple of 2π, and these transmission spectra

Optics EXPRESS

have the same FSR_e. Thus, unique spectral signature and extended effective free spectral range are achievable by means of the angular separation specified for a MARC device.

3. Design and fabrication

We designed MARC devices based on silicon strip waveguides with balanced MZIs and ring resonators, operating in the telecommunication wavelength band. Ring resonators were designed with a radius of 30 μm, a coupling gap between the ring and the bus waveguides of 150 nm, and five angular separations of 30°, 45°, 90°, 135°, and 180°. Silicon strip waveguides were 500 nm wide and 220 nm high to support the fundamental TE-like mode at the source wavelength of 1550 nm. For waveguide input and output coupling, inverted taper couplers were utilized to enhance the coupling efficiency.

MARC devices were fabricated on amorphous silicon-on-insulator (SOI) consisting of a hydrogenated amorphous silicon ($\alpha - Si : H$) layer of 220 nm and a buried thermal oxide layer of 1 μm on a 100 mm silicon wafer. The hydrogenated amorphous silicon was deposited by plasma enhanced chemical vapor deposition (PECVD). MARC devices were patterned by electron beam lithography (Elionix ELS-G100) using e-beam resist (Allresist AR-P 6200), followed by dry etching with inductively coupled plasma reactive ion etching (ICP-RIE). The fabricated devices were inspected under the scanning electron microscope (SEM). SEM images of fabricated devices with angular separations of 180° and 90° are shown in Fig. 4.

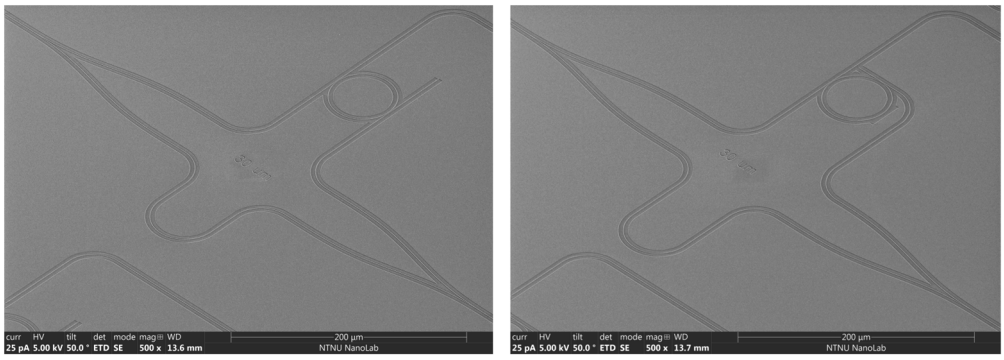

(a) (b)

Fig. 4. SEM images of the MARC with a ring radius of 30 μm and angular separations of (a) 180°, and (b) 90°.

4. Experimental characterization

For optical characterization and evaluation of the MARC devices, end-fire coupling between the input waveguides and the tapered lensed fiber having a working distance of 14 μm and a spot diameter of 2.5 μm was used. A tunable external cavity laser (Thorlabs TLK-L1550M) with 1550 nm center wavelength and a fiber polarization controller (Thorlabs FPC562) were used for controlling the wavelength and the input polarization of the light. Two single mode fibers were placed at the output waveguides: one for the through port and the other for the MARC output, and these fibers were directly connected to InGaAs photodetectors (Thorlabs DET10C2).

Figure 5 presents transmission spectra obtained from the fabricated MARC devices. This confirms the theoretical prediction that the MARC devices with different angular separations produce a variety of spectral signatures. The discrepancies between experimental spectra in Fig. 5 and the corresponding theoretical spectra in Fig. 3 are due to a combination of wavelength dependent laser power, waveguide fabrication imperfections, and interference from chip end facet

Optics EXPRESS

reflections. As can be seen in Fig. 5(c), the transmission spectrum from MARC with 90° angular separation consists of three distinct resonance lineshapes: Lorentzian, inverse Lorentzian and Fano-like resonance shapes, separated by the *FSR* of 2.95 *nm*. Due to its spectral signature, it shows the FSR_e of 11.8 *nm*, which is four times larger than the normal *FSR*. In the 45° case, the measured transmission spectrum exhibit five distinct resonance lineshapes including Lorentzian, inverse Lorentzian and three non-identical asymmetric Fano-like shapes (Fig. 5(d)). In addition to that, the measured FSR_e is 23.6 *nm*. The 135° case also shows five distinct resonance lineshapes and FSR_e of 23.6 *nm* as shown in Fig. 5(b). As predicted from the calculations, it is experimentally confirmed that spectra of 45° and 135° have the same FSR_e. In spite of the same FSR_e, these transmission spectra are very distinctive since each spectrum has unique spectral signatures over the operational wavelength band.

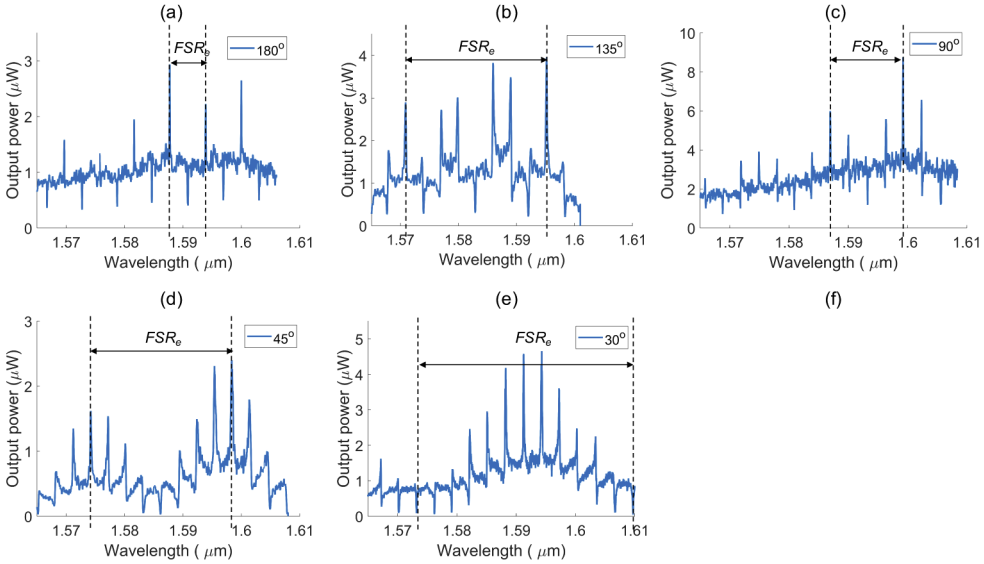

Fig. 5. Measured non-normalized transmission spectra of the MARC for angular separations of (a) 180°, (b) 135°, (c) 90°, (d) 45°, and (e) 30°.

5. Sensing experiment

To investigate a potential application of the spectral signature generated from a MARC device, we performed a temperature sensing measurement. We designed and fabricated several MARC devices with the angular separation of 180° and ring radii of 30 μm and 45 μm in order to determine the Q-factor and the sensing performance. In addition to that, although the coupling gap between the ring and the bus waveguide is a crucial parameter [21], the coupling gap is fixed to be 150 *nm* due to the fabrication process simplification. In this experiment, we monitor simultaneously both output signals from the through port and the MARC output.

The measured Q-factors are 29,600 and 51,900 for MARC devices with ring radii of 30 μm and 45 μm, respectively. These measurement values are averaged from four different MARC devices. The corresponding *FSR*s measured from the through port output are 2.95 *nm* and 1.88 *nm*, and FSR_es measured from the MARC output are 5.9 *nm* and 3.76 *nm* for ring radii of 30 μm and 45 μm, respectively. The transmission spectra from the through port and the MARC outputs of a 45 μm ring radius device are shown in Fig. 6(a). The MARC device with the ring radius of 45 μm has the highest Q-factor of 60,000 and FSR_e of 3.76 *nm* and was therefore selected for temperature sensing. For the temperature sensing experiment, the photonic chip was mounted on

Optics EXPRESS

the stage equipped with a Peltier element, and the temperature was varied from 21°C to 48°C while the optical outputs were continuously monitored. The 27°C rise in temperature causes the 2.5 *nm* red shift of the entire transmission spectrum as can be seen Fig. 6(b), which exceeds the *FSR* of 1.88 *nm*. This red shift, however, falls within the range of the FSR_e (3.76 *nm*), and consequently its measurement range is extended to the FSR_e. Therefore, it is demonstrated that the MARC sensor utilizing the FSR_e and the unique transmission spectrum has a 2-fold increase in the measurement range constrained generally by the *FSR* of conventional RR and MZI based sensors. Moreover, it is demonstrated that the increase in the ring radius from 30 μm to 45 μm to reduce the bending losses result in 75 % enhancement in the Q-factor with only 36 % reduction in the FSR_e. This FSR_e can be further enhanced by changing the angular separation. Thus, the MARC device with a large ring radius enables the realization of a sensor with both high Q-factor and wide measurement range.

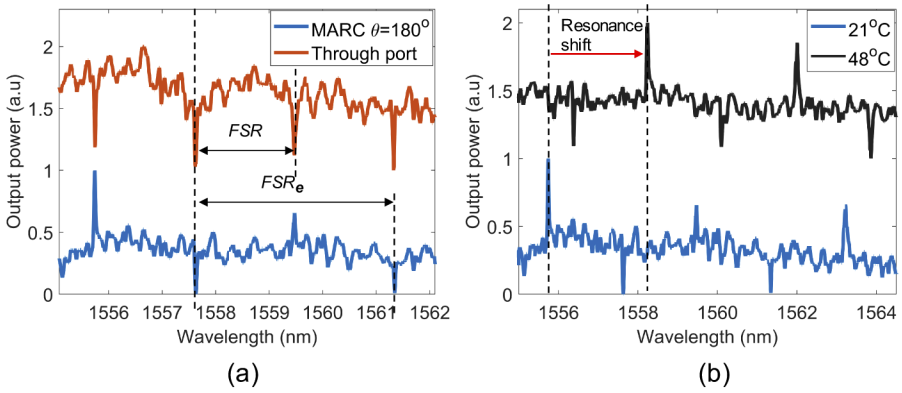

Fig. 6. (a) Measured transmission spectra from a MARC device with the ring radius of 45 um and the angular separation of 180°, (b) MARC transmission spectra at different temperatures. Noise in signals is likely due to reflections from end facets. Note: Offset in y direction is added to the plots to separate out transmission spectra.

6. Conclusion

We have proposed and experimentally demonstrated the Mach-Zehnder interferometer assisted ring resonator configuration (MARC), which generates transmission spectra with unique spectral signatures and significantly large effective free spectral ranges. It utilizes the angular separation between the through port and the drop port waveguides to realize spectral signatures. Spectral signatures generated from MARC are comprised of distinct resonance lineshapes including Lorentzian, inverse Lorentzian, and Fano-like lineshapes.

A temperature sensing experiment has been presented to exhibit a potential application of spectral signatures in optical sensing. It demonstrates that the measurement range of a ring resonator sensor can be enhanced by changing the angular separation between the drop port and the through port waveguides, instead of reducing the ring radius. In addition to enhancing the measurement range, spectral signatures can be used to label RRs with specific spectral fingerprints, which can potentially be utilized for multiplexing of RR sensors in a MARC.

The proposed MARC device can be designed to give any number of distinct resonance lineshapes within a narrow spectrum band, which could be desirable for optical switching and filtering.

Funding. Norges Forskningsråd (245963/F50, 248869/O70).

Optics EXPRESS

Acknowledgments. The Research Council of Norway is acknowledged for the support to the Lab-on-a-chip Biophotonic Sensor Platform for diagnostics, project number 248869/O70 and the Norwegian Micro- and Nano-Fabrication Facility, NorFab, project number 245963/F50. The authors would like to thank Jens Høvik from Department of Electronic Systems, NTNU for fruitful discussions.

Disclosures. M.Y., A.A. and D.R.H. have applied for patent GB2004009.3 for optical sensing apparatus. The other author declares no competing financial interests.

References

1. G. Griffel, "Synthesis of optical filters using ring resonator arrays," IEEE Photonics Technol. Lett. **12**(7), 810–812 (2000).
2. B. E. Little, S. T. Chu, H. A. Haus, J. Foresi, and J.-P. Laine, "Microring resonator channel dropping filters," J. Lightwave Technol. **15**(6), 998–1005 (1997).
3. M. R. Watts, W. A. Zortman, D. C. Trotter, R. W. Young, and A. L. Lentine, "Vertical junction silicon microdisk modulators and switches," Opt. Express **19**(22), 21989–22003 (2011).
4. H. M. Robison and R. C. Bailey, "A guide to quantitative biomarker assay development using whispering gallery mode biosensors," Curr. protocols chemical biology **9**(3), 158–173 (2017).
5. T. Claes, J. G. Molera, K. De Vos, E. Schacht, R. Baets, and P. Bienstman, "Label-free biosensing with a slot-waveguide-based ring resonator in silicon on insulator," IEEE Photonics J. **1**(3), 197–204 (2009).
6. C. F. Carlborg, K. B. Gylfason, A. Kaźmierczak, F. Dortu, M. J. Bañuls, A. Maquieira Catala, G. M. Kresbach, H. Sohlström, T. Moh, L. Vivien, J. Popplewell, G. Ronan, C. A. Barrios, G. Stemme, and W. van der Wijngaart, "A packaged optical slot-waveguide ring resonator sensor array for multiplex label-free assays in labs-on-chips," Lab Chip **10**(3), 281–290 (2010).
7. T. Claes, W. Bogaerts, and P. Bienstman, "Experimental characterization of a silicon photonic biosensor consisting of two cascaded ring resonators based on the vernier-effect and introduction of a curve fitting method for an improved detection limit," Opt. Express **18**(22), 22747–22761 (2010).
8. A. Ksendzov and Y. Lin, "Integrated optics ring-resonator sensors for protein detection," Opt. Lett. **30**(24), 3344–3346 (2005).
9. W. Bogaerts, R. Baets, P. Dumon, V. Wiaux, S. Beckx, D. Taillaert, B. Luyssaert, J. V. Campenhout, P. Bienstman, and D. V. Thourhout, "Nanophotonic waveguides in silicon-on-insulator fabricated with cmos technology," J. Lightwave Technol. **23**(1), 401–412 (2005).
10. Y. Lu, J. Yao, X. Li, and P. Wang, "Tunable asymmetrical fano resonance and bistability in a microcavity-resonator-coupled mach–zehnder interferometer," Opt. Lett. **30**(22), 3069–3071 (2005).
11. S. Darmawan, Y. Landobasa, and M. Chin, "Phase engineering for ring enhanced mach-zehnder interferometers," Opt. Express **13**(12), 4580–4588 (2005).
12. R. A. Cohen, O. Amrani, and S. Ruschin, "Response shaping with a silicon ring resonator via double injection," Nat. Photonics **12**(11), 706–712 (2018).
13. Y. Zhang, S. Darmawan, L. Tobing, T. Mei, and D. Zhang, "Coupled resonator-induced transparency in ring-bus-ring mach-zehnder interferometer," J. Opt. Soc. Am. B **28**(1), 28–36 (2011).
14. C.-Y. Chao and L. J. Guo, "Biochemical sensors based on polymer microrings with sharp asymmetrical resonance," Appl. Phys. Lett. **83**(8), 1527–1529 (2003).
15. Y. Yu, M. Heuck, H. Hu, W. Xue, C. Peucheret, Y. Chen, L. K. Oxenløwe, K. Yvind, and J. Mørk, "Fano resonance control in a photonic crystal structure and its application to ultrafast switching," Appl. Phys. Lett. **105**(6), 061117 (2014).
16. M. F. Limonov, M. V. Rybin, A. N. Poddubny, and Y. S. Kivshar, "Fano resonances in photonics," Nat. Photonics **11**(9), 543–554 (2017).
17. L. Zhou and A. W. Poon, "Fano resonance-based electrically reconfigurable add-drop filters in silicon microring resonator-coupled mach-zehnder interferometers," Opt. Lett. **32**(7), 781–783 (2007).
18. H.-W. Chen, A. W. Fang, J. D. Peters, Z. Wang, J. Bovington, D. Liang, and J. E. Bowers, "Integrated microwave photonic filter on a hybrid silicon platform," IEEE Trans. Microwave Theory Tech. **58**(11), 3213–3219 (2010).
19. F. Wan, G. Qian, R. Li, J. Tang, and T. Zhang, "High sensitivity optical waveguide accelerometer based on fano resonance," Appl. Opt. **55**(24), 6644–6648 (2016).
20. B. Troia, J. S. Penades, Z. Qu, A. Z. Khokhar, A. Osman, Y. Wu, C. Stirling, M. Nedeljkovic, V. M. Passaro, and G. Z. Mashanovich, "Silicon ring resonator-coupled mach–zehnder interferometers for the fano resonance in the mid-ir," Appl. Opt. **56**(31), 8769–8776 (2017).
21. W. Bogaerts, P. De Heyn, T. Van Vaerenbergh, K. De Vos, S. Kumar Selvaraja, T. Claes, P. Dumon, P. Bienstman, D. Van Thourhout, and R. Baets, "Silicon microring resonators," Laser Photonics Rev. **6**(1), 47–73 (2012).
22. Y. Zhang, K. Wang, X. Liu, and X. Zhang, "An add-drop ring resonator interferometer sensor with high sensitivity," in *2013 Seventh International Conference on Sensing Technology (ICST)*, (2013), pp. 316–319.